3.2.3 OTSK13

1 Algorithm Outline

1. Algorithm Code: OTSK13
2. Product Code: SST, QF_ST
3. PI names: G-0068 Hiroshi Kawamura
4. Overview of algorithm (Standard level)

   The GLI Sea Surface Temperature (SST) algorithm contains the following two process: the cloud detection and the atmospheric correction. The former is a process to find clear, or no cloud-contaminated, pixels in the image. The latter is need to obtain SST of clear pixels from the brightness temperatures observed by GLI. Accurate SST retrieval depends on the success of these processes.

   As for the cloud detection, the combination of the threshold tests is used to detect clouds. A pixel, which passes through all the tests, is flagged as clear. The tests need to set coefficients and thresholds; they are adjusted using the real GLI data after the launch of ADEOS-II.

   As for the atmospheric correction, the Multi-Channel SST (MCSST) technique is used. The radiative transfer model and the match-up dataset are used to determine the coefficients of the MCSST equation. The methodology follows in that done in OCTS SST retrieval (Sakaida et al., 1998)

2 Algorithm Description

2.1 Methodology and Logic flow

The whole process is summarized in the following chart (Fig.1). As mentioned above, the GLI SST products are obtained through the cloud detection and the atmospheric correction. The detail of each process will be described later.

As shown in Figure 1, the SST data (SST) and the quality flag data (QF_ST) are produced using the GLI data and the climatological SST data. As for the GLI data, the following 10 bands are used: Band-8(0.545μm), -13(0.678μm), -19(0.865μm), -26(1.24μm), -27(1.38μm), -30(3.7μm), -31(6.7μm), -34(8.6μm), -35(10.8μm), and -36(12μm). The radiances are converted to reflectance,R, for visible and near infrared band (band 8-27), brightness temperature, BT, for thermal infrared band (band 30-35). CLFLG_p (Ackerman's cloud mask data) is also needed. As for ancillary data, the climatological SST data are needed for the quality control (QC). The specification of QF_ST is shown in the following table (Table 1). QF_ST is partly filled in the cloud detection process and the atmospheric correction process and is complemented after these processes.

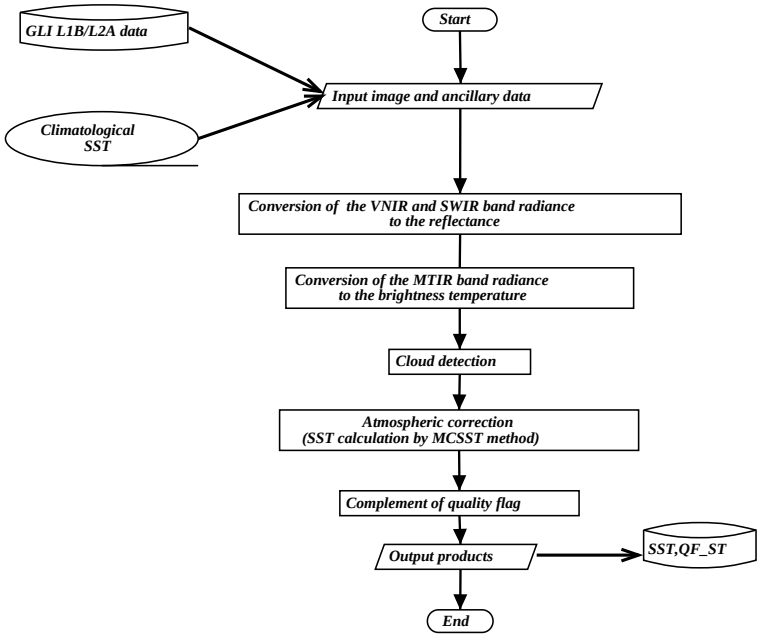

Figure 1: The flowchart of the whole process of OTSK13.

Table 1: The specification of the GLI SST flag data.

BIT FIELD	Description Key	Result
1	Land/Sea	0=Sea/1=Land
2	Cloud	0=Clear/1=Cloudy
3	Lack of observation	0=No/1=Yes
4	Large emission angle [1]	0=No/1=Yes
5	Out of valid range [2]	0=No/1=Yes
6	Day/Night	0=Day/1=Night
7	Sun glint	0=No/1=Yes
8	Forward tilt	0=No/1=Yes
9	Backward tilt	0=No/1=Yes
10-11	Ackerman's four cloud class	00 = cloudy 01 = probably cloud 10 = confident clear 11 = high confidence clear
12-16	Spare	

[1] The threshold of scan angle is 55°.

[2] The threshold of the difference between GLI SST and climatological SST is standard deviation of climatological SST.

2.2 Cloud detection algorithm

The framework of cloud detection algorithm is to apply up to some threshold tests and then to identify a pixel as cloud-free when all tests prove negative. Figure 2 shows processing flow of the cloud detection. We use "scheme" to represent the combination of cloud detection tests. Scheme-3 (nighttime) cloud detection algorithms are used when the solar zenith angle θ_{suz} is greater than θ_{a0} = 86.5°.

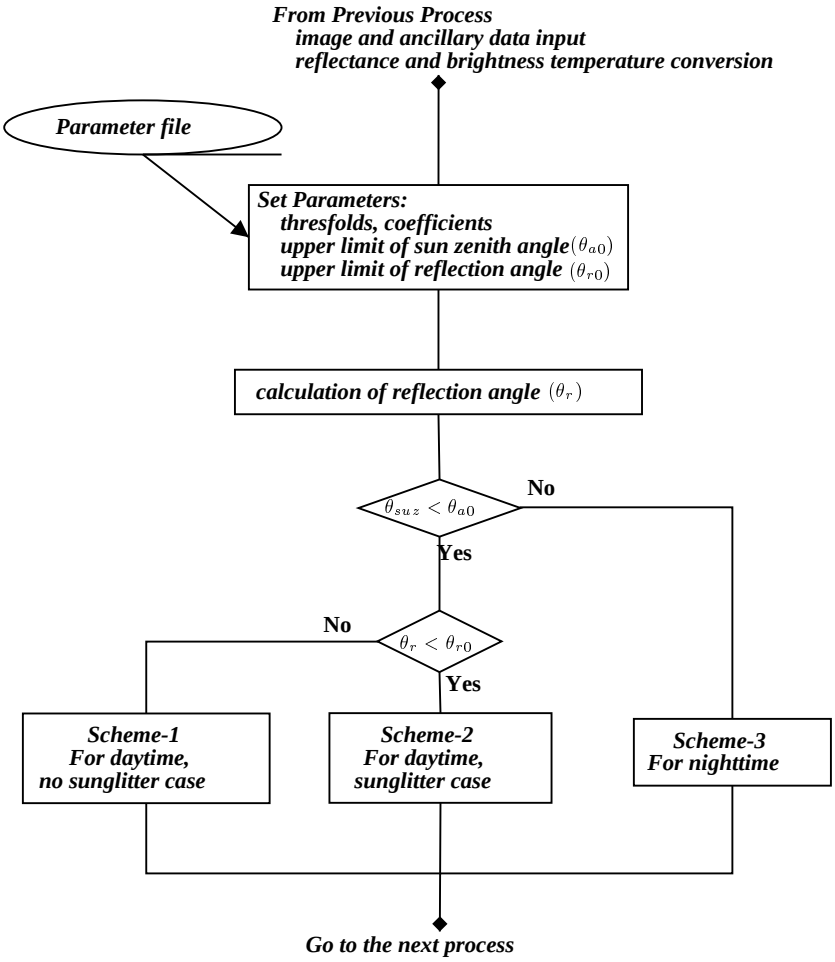

Figure 2: The processing flow of the cloud detection.

In the daytime, scheme-1 algorithms apply to the exterior of the sunglitter; scheme-2 are used to sunglitter region. To specify the sunglitter region, the reflection angle, θ_r, is used. θ_r is calculated by,

$$\cos\theta_r = \frac{\cos\theta_{suz} + \cos\theta_{saz}}{2\cos\omega}, \tag{1}$$

where ϕ_{saz} is satellite zenith angle. ω can be derived by,

$$\begin{aligned}\cos 2\omega &= \cos\theta_{saz}\cos\theta_{suz} \\ &\quad - \sin\theta_{suz}\theta_{saz}\cos(\phi_{sua} - \phi_{saa}),\end{aligned} \tag{2}$$

where ϕ_{sua} and ϕ_{saa} are the azimuthal angles of the sun and the satellite, respectively. This geometry

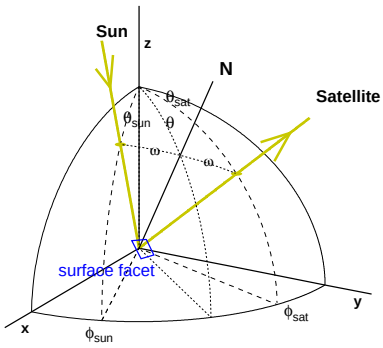

Figure 3: The reflection geometry between the sun, the satellite, and the surface facet.

is shown in Figure 3. The limit value θ_{r0} for specifying sunglitter region is 30 degree. It is determined empirically as will be explained later.

Table 2 shows the cloud detection tests used in GLI SST. These tests are classified to four groups as follows.

The first group is called as a gross cloud test. A pixel is flagged as cloudy when the brightness temperature of band-35 (10.8μm) is lower than the thresfold value. Tanahashi et al. (2000) used quadratic function of latitude as the thresfold value for S-VISSR/GMS. We adopted their forms with coefficients derived from GLI data empirically. Constant thresfold is used in conjection with quadratic function to identify clouds in high latitude regions.

The second tests use visible and near-infrared reflectance (R). These tests are widely used for retrieving SST from visible and infrared radiometer (e.g., Saunders and Kriebel, 1988; Ackerman et al., 1997; Sakaida et al., 2000). Reflectance ratio tests utilize the difference in reflection from cloud versus earth surface in wavelength above and below 0.72μm (Ackerman et al., 1997). Early studies used the 0.87μm reflectance divided by 0.66μm reflectance ($R_{0.87}/R_{0.66}$). Based on GLI data, it is found that $R_{0.865}/R_{0.545}$ (band-19 reflectance divided by band-8 reflectance of GLI) is more efficient for classifying cloud and ocean than $R_{0.865}/R_{0.678}$ (band-19 reflectance divided by band-13 reflectance). Figure 4 shows the scatter diagrams of $R_{0.865}/R_{0.545}$ and $R_{0.865}/R_{0.678}$ from GLI data. It reveals that the former can distinguish the clear ocean from cloudy even in the sunglitter region. In order to avoid the potential for masking clear pixels in sunglitter region, the linear theresfold function and sunglitter region ($\theta_r < 30$degree) are defined empirically. Reflectance test for band-19 ($R_{.865}$) is used additinally and the thresfold is determined as a function of reflection angle empirically.

The third tests are brightness temperature difference (BTD) tests. The test using BTD between 11μm(band-35:10.8μm) and 12μm (band-36) is widely known as split window method, which is useful for detecting relatively thin clouds. It is known that the BTD depends on the brightness temperature of 11 μm (BT_{11}). Saunders and Kriebel (1988) defined the thresfold as a function of satellite zenith angle and BT_{11} for AVHRR/NOAA. Stowe et al. (1999) suggested the 5-th order function of BT_{11} as the thresfold for cloud classfication from AVHRR/NOAA. Based on these reserches and the GLI data, the thresfold function for GLI is determined as exponential function of $BT_{10.8}$ (band-35) empirically. In addition, to avoid the striping noise and masking the frontal region, BTD is averaged

Table 2: Cloud detection tests for GLI-SST. The tests checked by ∘ are used in each scheme. Scheme-1: Daytime, outside the sun glint region. Scheme-2: Daytime, in the sun glint region. Scheme-3: Nighttime. BT_α:Brightness temperatures at $\alpha\mu$m, R_α:reflectance at $\alpha\mu$m, ϕ: latitude, θ_r: reflection angle, ∇_{mn}: Max-Min difference in 3x3 box, ∇_{mv}: Max-Center pixel value difference in 3x3 box. Overline on $BT_{10.8} - BT_{12}$ denotes the mean in 3x3 box except for maximum value. FR: Full Resolution product, LR: Low Resolution product.

Group	Cloud detection test	Scheme		
		1	2	3
Gross test	$BT_{10.8} \leq -0.007\phi^2 + 283$	∘	∘	∘
	$BT_{10.8} \leq 269.15$	∘	∘	∘
Reflectance test	$R_{0.865}/R_{0.545} > 1.05 - 0.019\theta_r$	×	∘	×
	$R_{0.865}/R_{0.545} > 0.48$	∘	×	×
	$R_{0.865} > 30.0 - .50\theta_r$	×	∘	×
	$R_{0.865} > 15.0$	∘	×	×
	$R_{1.38} > 0.2$ and $R_{0.865}/R_{0.545} > 0.4$	∘	∘	×
BTD test	$BT_{8.6} - BT_{10.8} > -0.5$	∘	∘	∘
	$\overline{BT_{10.8} - BT_{12}} > \exp(0.176BT_{10.8} - 50.5) + 1.45$	∘	∘	∘
	$\overline{BT_{10.8} - BT_{12}} > 4.3$	∘	∘	∘
	$1.5BT_{3.7} - 2.5BT_{10.8} + BT_{12} > 3.5$	×	×	∘
	$1.5BT_{3.7} - 2.5BT_{10.8} + BT_{12} < -2.5$	×	×	∘
	$0.6BT_{3.7} - 0.6BT_{8.6} + BT_{10.8} - BT_{12} < 1.8$	×	×	∘
	$BT_{3.7} - BT_{12} \leq \exp(0.0345BT_{10.8} - 9.375) + 1.$	×	×	∘
Uniformity test	$\nabla_{mv}BT_{10.8} > 1.5$ and $\nabla_{mn}(BT_{10.8} - BT_{12}) > 2.5$	∘	∘	∘
	$\nabla_{mn}R_{1.24} > 2.5$	∘	∘	×
	$\nabla_{mn}BT_{3.7} > 1.25$(FR) 2.0 (LR)	×	×	∘

over 3x3 pixel box except for maximum value. The test using BTD betwenn 8.6μm (band-34) and 10.8μm (band-35) is also useful to detect cloud. It is known that this BTD indicates ice cloud (Strabara et al., 1994). Since the dependency on the BT_{11} is weak, the thresfold of this test is determined as constant value. For nighttime observation, BTDs between 3.7μm (band-30) and other bands are used as cloud detection tests. Stowe et al. (1999) used BTD between 3.7μm and 12μm with a thresfold function of BT_{11} for nighttime test. Sakaida et al. (2000) and Guan et al. (2003) used the combination of $BT_{3.7}, BT_{11}$ and BT_{12} to detect cloud in nighttime. The combination of $BT_{3.7}$, $BT_{8.6}$, $BT_{10.8}$ and BT_{12} is useful for detectinl low-level cloud in high latitude regions. The coefficients of these tests are adjusted to GLI data.

The forth tests are uniformity tests, which is based on the fact that brightness temperatures and reflectances on clear ocean are spatially homogeneous compared with cloudy regions. While these

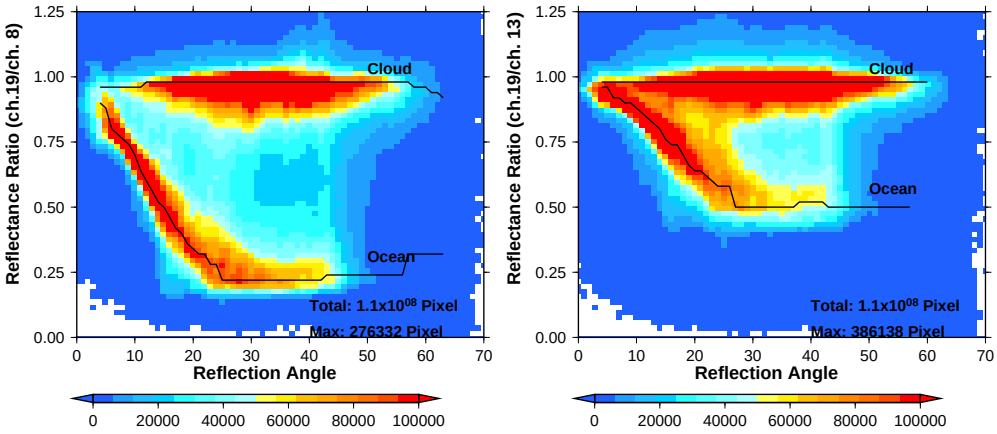

Figure 4: Scatter diagram of reflectance ratio and reflection angle based on GLI data. (Left) $R_{0.865}/R_{0.545}$ (band-19 reflectance divided by band-8 reflectance), (Right) $R_{0.865}/R_{0.678}$ (band-19 reflectance divided by band-13 reflectance). Color shows the frequency of appearance.

tests are very powerful, its reliability is low in the coastal and frontal regions. Since the tendency for cloudy condition is colder than clear condition, uniformity of $BT_{10.8}$ (band-35) is confirmed by the brightness temperature difference between maximun in 3x3 pixel box and the center pixel value, which is used in Rossow and Garder (1993). In addition, the uniformity of BTD ($BT_{10.8} - BT_{12}$) is combined to avoid masking the frontal region as cloud. The uniformity of BTD and reflectance are calculated by maximum and minumum difference in 3x3 pixel box. For nighttime, uniformity of $BT_{3.7}$ (band-30) is used. Thresfold for $BT_{3.7}$ uniformity test is changed as FR (full-resolution) and LR (low-resolution), since noise at GLI band-30 is so large that the spatial homogeneity of $BT_{3.7}$ in clear region of LR is less than that in FR. These thresfolds are determined empirically.

2.3 Atomospheric correction

In the GLI SST product, the MCSST method is used to retrieve the SST in clear pixels. The MCSST equation is the same form as one used in OCTS/ADEOSS SST algorithm (Sakaida et al., 1998) as follows:

$$\begin{aligned} SST &= a_1 + a_2 BT_{10.8} + a_3 \overline{BT_{10.8} - BT_{12}} + a_4 \overline{BT_{10.8} - BT_{8.6}} \\ &\quad + a_5 \overline{BT_{10.8} - BT_{12}} (1/\cos(\theta_{saz}) - 1.0) \\ &\quad + a_6 \overline{BT_{10.8} - BT_{8.6}} (1/\cos(\theta_{saz}) - 1.0) \end{aligned} \tag{3}$$

where θ_{saz} is a satellite zenith angle.

The above equation contains $BT_{8.6}$, which is not observed by the split-window bands. The reason of this is that the use of this band is possibly advanced in the accuracy of SST

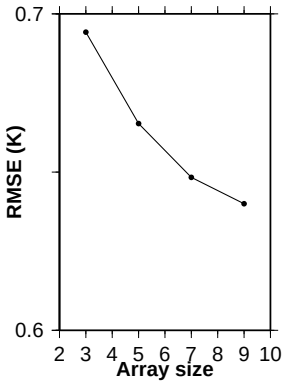

Figure 5: Residual of regression as a function of array size where brightness temperature differences are averaged.

estimation according to the study of OCTS and the numerical simulation (Moriyama et al., 1999). To reduce the noise effects, brightness temperature difference terms, $BT_{10.8} - BT_{8.6}$ and $BT_{10.8} - BT_{12}$. are averaged for NxN pixel array. The following chart (Fig. 6) shows the SST calculation process with the detail of this averaging.

Using GOES data, Wu et al. (1999) pointed out that the optimal box size of averaging brightness temperature differences is as small as 3x3 array for representative of a buoy measurement, since the RMSE (root-mean-square-error) of satellite-estimated and buoy-measured SSTs is minimum using 3x3 array averaging. From GLI data, RMSE between GLI-estimated and buoy-measured SST (observation points are shown in Figure 8) monotonically decreases with array size (Fig.5). Since RMSE difference of 7x7 array and 9x9 array is small, it is suggested that 7x7 array is optimal for GLI SST. Figure 6 shows the chart of SST calculation process.

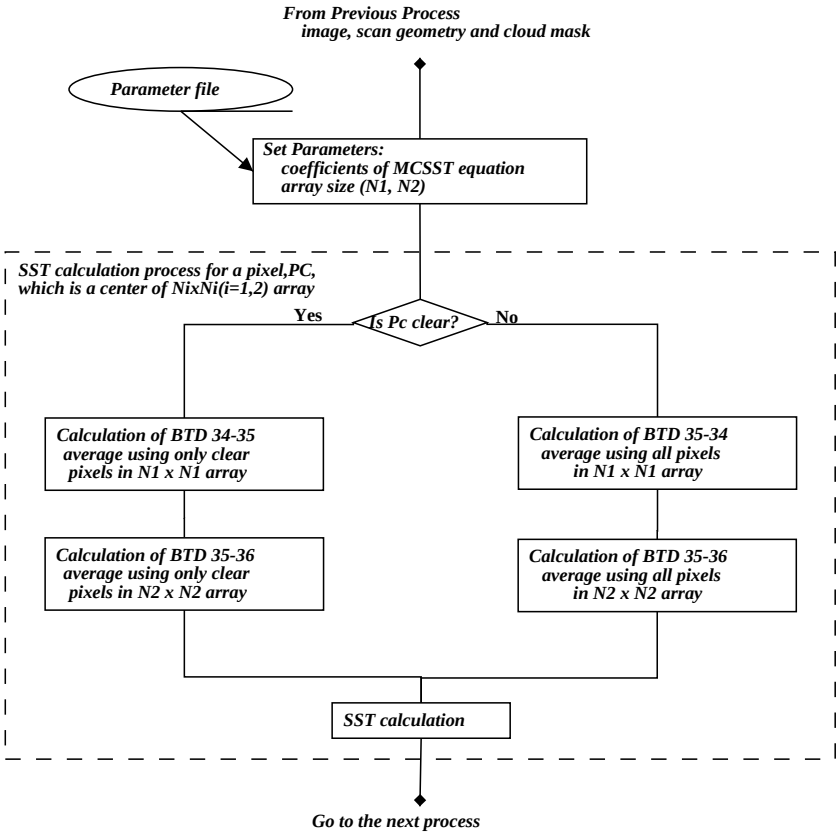

Figure 6: The SST calculation process with the detail of this averaging.

The coefficients of Eq.(3) are derived by the pre-launch numerical simulation (see Section A). The MCSST equation (pre-launch) is written as,

$$\begin{aligned} SST &= 2.276 + 0.9966BT_{10.8} + 1.946\overline{BT_{10.8} - BT_{12}} - 0.2106\overline{BT_{10.8} - BT_{8.6}} \\ &\quad +0.507\overline{BT_{10.8} - BT_{12}}(1/\cos(\theta_{saz}) - 1) \\ &\quad +0.2481\overline{BT_{10.8} - BT_{8.6}}(1/\cos(\theta_{saz}) - 1) \end{aligned} \tag{3-a}$$

After the launch of the ADEOS-II, the match-up data are collected. Using the match-up data, the

coefficients of Eq.3 are also derived. The equation is written as,

$$\begin{aligned} SST &= -2.35069 + 1.019241 BT_{10.8} + 1.863587\overline{BT_{10.8} - BT_{12}} - 1.11811\overline{BT_{10.8} - BT_{8.6}} \\ &\quad +1.020815\overline{BT_{10.8} - BT_{12}}(1/\cos(\theta_{saz}) - 1) \\ &\quad +0.272058\overline{BT_{10.8} - BT_{8.6}}(1/(\cos\theta_{saz}) - 1) \end{aligned} \tag{3-b}$$

In the calculation of this equation coefficient, the match-up data in 3/19-22 and 4/2-7 are used. The number of the match-up data is 546. In the match-up data used to derive Eq.(3-b), the time difference between the satellite and in-situ observation is within 2 hours.

Using the same data that Eq.(3-b) is derived, RMSE and bias are calculated for the equations (3-a) and (3-b). The RMSE of Eq.(3-b) is 0.56K. For Eq.(3-a), the RMSE is 0.66K and the bias is -0.16K. The RMSEs and biases of the equations (3-a) and (3-b) are also calculated using the data independent of the coefficient calculation. Using the 1732 match-up data in 5/28-31, Eq.(3-a) has the RMSE of 0.69K and the bias of -0.16K and Eq.(3-b), the RMSE of 0.62K and the bias of 0.06K. Therefore, we adopt Eq.(3-b) as the equation for the GLI SST retrieval.

3 Validation

For validating the SST product from OTSK13, mutchup data of GLI-estimated SST and buoy-measured SST are used. Buoy observation is quality checked using climatological SST. The mutchup is collected from 22 days (randomly selected from March to September), if time difference between buoy and GLI observations is less than 5 hours. Figure 7 shows that the GLI SST residual decreases with an increasing number of clear pixels around the buoy. This is consistent with the fact that the cloud contamination and atmospheric correction failure are occasional near cloud area. Through the quality control in which more than 8 pixels in 3x3 array around the point are clear, number of mutchup is 4225.

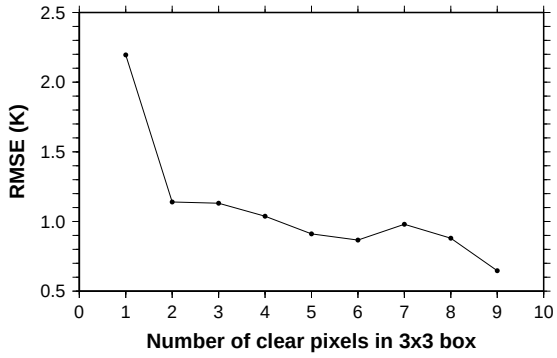

Figure 7: RMSE as a function of the number of clear pixels in 3x3 box.

Figure 8 shows the mutchup measurements points and scatter diagram of GLI and buoy SST. The bias and RMSE of the difference between GLI and buoy SST are -0.08K and 0.672K, respec-

tively. They are -0.06K and 0.669K for daytime, while they are -0.17K and 0.69K for nighttime. The seasonal or temporal change of statistical features is not found.

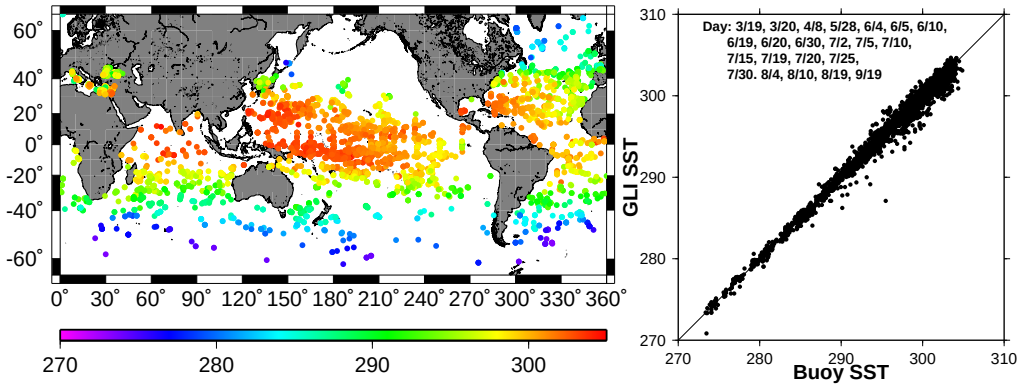

Figure 8: (Left)Location of the mutchups. Color denotes the buoy measurement SST. (Right) Comparison of GLI estimated SST and buoy measurements.

Appendix

A Physical and Mathematical aspects of the algorithm based on radiative transfer model

The coefficients of the split-windows equation will be defined from the multivariative regression using the match-up dataset which has the satellite detected brightness temperature and the scan geometry collocated with the sea surface temperature which are measured by buoys, ships, aircrafts and so on. For the initial definition of the split-window formula, it is desireable to define the function type which can make the stable estimation under the real observation.

For the Global mapping, the error of the estimated SST must be independent from the observed brightness temperature. The following is the mathematical expression of this concept,

$$\delta_T = \sum \frac{df}{dT_i} \delta T_i \tag{4}$$

where δ_T, f and δT_i are the error of the estimated SST, the split-window function and the observation error of the brightness temperature of ith spectral channel respectively. The partial derivative of the split-window function is constant when the split-window function is linear, so that the estimation error of the SST will be independent from the brightness temperature. From this reason, the GLI split-window function is defined as the linear function.

For the function type definition, the numerical simulation, which is based on the model atmosphere/surface conditions, is described as follows.

- Model atmosphere: 1990 Monthly mean NCEP dataset, Longditudal averaged over 10 [deg.] latitude
- interval (12 x 18 = 216)
- Other gas amount: NRL model
- Model SST: T(0) + 1 [K] + normal random variable with 5/3 [K] standard deviation.
- observation zenith: 0, 30, 60 [deg.]
- Radiative transfer code: MODTRAN 3.5
- Computation item: brightness temperature at GLI 34, 35, 36channels.
- Observation error: Normal random variable with 0, 0.1, 0.2 [K] standard deviation.
- Aerosol type: Rural
- Aerosol amount: Surface visibility: 23 [km] (@550nm)
- Model emissivity: 1.0, 0.99, 0.98, 0.97

From these conditions, the brightness temperature at GLI channels 34, 35 and 36 are computed. By using the above dataset, the multivariative regression analysis based in the following formulae are made.

$$SST = aBT_{10.8} + b(BT_{10.8} - BT_{12}) + f \quad (5)$$

$$SST = aBT_{10.8} + b(BT_{10.8} - BT_{12}) + c(BT_{10.8} - BT_{8.6}) + f \quad (6)$$

$$SST = aBT_{10.8} + b(BT_{10.8} - BT_{12}) + c(BT_{10.8} - BT_{8.6}) + d(BT_{10.8} - BT_{12})(1/\cos(\theta_{saz}) - 1.0) + f \quad (7)$$

$$SST = aBT_{10.8} + b(BT_{10.8} - BT_{12}) + c(BT_{10.8} - BT_{8.6}) + d(BT_{10.8} - BT_{12})(1/\cos(\theta_{saz}) - 1.0) + e(BT_{10.8} - BT_{8.6})(1/\cos(\theta_{saz}) - 1.0) + f \quad (8)$$

The RMS error of the estimated SST under the no observation error case from the above formulae are listed below

Eq.	(5)	(6)	(7)	(8)
RMSE(K)	0.559	0.312	0.424	0.291

The Equation (8) show the most accurate result, so that this function type (5 terms formula) is used for the GLI split-window formula.

As the preliminary set of the coefficients are defined from the following scheme.

1. The coefficient sets are defined from the common observation error and the surface emissivity.
2. Compute the RMS error of the estimated SST from the all brightness temperature data based on each coefficient set.
3. The coefficient set which minimize the RMS error is selected as the preliminary set.

Bias and RMS error from the each coefficient set are listed below.

ϵ	0.97			0.98		
$NEdT$	0.0	0.1	0.2	0.0	0.1	0.2
RMS(K)	0.634702	1.0413	1.34708	0.56707	0.816566	0.969785
ϵ	0.99			1.00		
$NEdT$	0.0	0.1	0.2	0.0	0.1	0.2
RMS(K)	0.582015	0.743614	1.20846	0.659112	1.0384	1.25814

From the RMS error, the coefficient set for the condition, in which the surface emissivity is 0.99 and the observation noise is 0, are selected. The preliminary coefficient set is as follows. a = 0.9966, b = 1.946 , c = -0.2106, d = 0.5070, e = 0.2481, f = 2.276

B Variables in parameter file

B.1 Cloud detection algorithm

The cloud detection tests shown in Table 2 are rewritten in the program as following inequalities:

$$\sum \alpha_j \chi > \gamma_a \quad \text{and} \quad \sum \beta_j \chi > \gamma_b, \tag{9}$$

where α_j and β_j are the coefficients, γ_a and γ_b are the thresholds, χ_j are variables. α_j, β_j, γ_a and γ_b are defined in parameter file as XALPHA, XBETA and XGAMMA. Table 3 shows the description of variables (data/aux/glisst_FR.prm).

Table 3: The variables for the cloud detection. Uniformity A and B are indices to measure the spatial variability. The 19th, 20th and 21th variables are used as $a_3 \exp(a_1 BT_{10.8} + a_2)$. Overline on brightness temperature difference (No.24 and No.25) denotes the mean in 3x3 box except for maximum value.

No.	Description
1	Uniformity test A
2	Uniformity test B
3	Reflectance of band-8 ($R_{0.545}$)
4	Reflectance of band-13 ($R_{0.678}$)
5	Reflectance of band-19 ($R_{0.865}$)
6	Reflectance of band-26 ($R_{1.24}$)
7	Reflectance of band-27 ($R_{1.38}$)
8	Brightness temperature of band-30 ($BT_{3.7}$)
9	Brightness temperature of band-31 ($BT_{6.7}$)
10	Brightness temperature of band-34 ($BT_{8.6}$)
11	Brightness temperature of band-35 ($BT_{10.8}$)
12	Brightness temperature of band-36 (BT_{12})
13	square of Latitude (ϕ^2)
14	Longitude
15	cosine of sun zenith angle $\cos\theta_{suz}$
16	1 minus secant of satellite zenith angle $1 - \sec\theta_{saz}$
17	product of reflection angle and $R_{0.545}$ $\theta_r \times R_{0.545}$
18	Ackerman's Cloud Flag
19	coefficient for exp($BT_{10.8}$) equation (a_1)
20	coefficient for exp($BT_{10.8}$) equation (a_2)
21	coefficient for exp($BT_{10.8}$) equation (a_3)
22	Reflection angle θ_r
23	$BT_{10.8} \times BT_{12}$
24	$\overline{BT_{10.8} - BT_{12}}$
25	$\overline{BT_{8.6} - BT_{10.8}}$

Band used in spatial uniformity tests is defined as XUNI CHN in the parameter file. XUNI CHN A and XUNI CHN B are for brightness temperature or reflectance tests, and XUNI CHN A0 and XUNI CHN B0 are for brightness temperature difference tests. The type of uniformity tests are selected by XUNI TYP parameters from following lists.

Table 4: The type of uniformity tests for R (reflectance or brightness temperature) at i, j pixel. il and jl mean the line and pixel lag ($il = -1, 0, 1$ and $jl = -1, 0, 1$). R_{max} and R_{min} are the maximum and minimum of R in 3x3 box, respectively.

parameter	description	equation
1	Difference of maximum and minimum in 3x3 box	$R_{Max} - R_{Min}$
2	Standard deviation	$\sum_{il,jl} R^2_{i+il,j+jl}/9 - (\sum_{il,jl} R_{i,j}/9)^2$
3	Spatial gradient	Maximum component of $\nabla R_{i,j}$
4	Laplacian	$\lvert\nabla^2 R_{i,j}\rvert$
5	Difference of maximum and the value at center pixel in 3x3 box	$R_{Max} - R_{i,j}$
6	Difference of minimum and the value at center pixel in 3x3 box	$R_{i,j} - R_{Min}$
7	Mean in 3x3 box except for maximum	$(\sum_{il,jl} R_{i+il,j+jl} - R_{Max})/8$

B.2 MCSST calculation

Table 5 explains the variables for MCSST equation in parameter file, in which these variables are separately defined for each regions (nighttime, daytime/sunglitter, daytime/out of sunglitter).

Table 5: Variables for MCSST calculation defined in parameter file.

Column 1	Description	Value in Ver. 1.0
XMCSST VAR	The number of the terms in the MCSST equation	6
XARRAY	array size to average the BTD.	
	XARRAY1 for BTD of band-34 and band-35	7 7
	XARRAY2 for BTD of band-35 and band-36	7 7
XCOEFF	coefficients for MCSST equation.	
	XCOEFFα ($\alpha = 1, ..., 6$) corresponds to a_α in Eq. (3).	(same as in Eq. (3-b))

References

Ackerman, S. A., K. Strabala, W. P. Menzel, R. A. Frey, C. C. Moeller, L. E. Gumley, B. A. Baum, C. Shaaf, and G. Riggs, 1997: Discriminating clear sky from cloud with MODIS algorithm theoretical basis ducument (MOD35). Eos ATBD web site,125pp.

Guan, L., H. Kawamura, and H. Murakami, 2003: Retrieval of sea surface temperature from TRMM VIRS. *J. Oceanogr.*, **59**, 245–249.

Moriyama, M., F. Sakaida, and H. Kawamura, 1999: Characteristics of 8μm band in terms of the global sea surface temperature retrieval, (in preparation).

Rossow, W. B. and L. C. Garder, 1993: Cloud detection using satelite measurements of infrared and visible radiance for ISCCP. *J. Clim.*, **6**, 2341–2369.

Sakaida, F., J.-I. Kudoh, and H. Kawamura, 2000: A-HIGHERS–The system to produce the high spatial resolution sea surface temperature maps of the western North Pacific using the AVHRR/NOAA. *J. Oceanogr.*, **56**, 707–716.

Sakaida, F., M. Moriyama, H. Murakami, H. Oaku, Y. Mitomi, A. Mukaida, and H. Kawamura, 1998: The sea surface temperature product algorithm of the Ocean Color and Temperature Scanner (OCTS) and its accuracy. *J. Oceanogr.*, **54**, 437–442.

Saunders, R. W. and K. T. Kriebel, 1988: An improved method for detectiong clear sky and cloudy radiance from AVHRR data. *Int. J. Remote Sensing*, **9**, 123–150.

Stowe, L. L., P. Davis, and E. P. McClain, 1999: Scientific basis and initial evaluation of the CLAVR-1 global clear/cloud classification algorithm for the Advanced Very High Resolution Radoimeter. *J. Atmos. Oceanic Technol.*, **16**, 656–681.

Strabara, K. I., S. A. Ackerman, and W. P. Menzel, 1994: Cloud properties inferred from 8–12-μm data. *J. App. Meteor.*, **33**, 212–229.

Tanahashi, S., H. Kawamura, T. Matsuura, T. Takahashi, and H. Yusa, 2000: Improved estimate of wide-ranging sea surface temperature from GMS S-VISSR data. *J. Oceanogr.*, **56**, 345–358.

Wu, X., W. P. Menzel, and G. S. Wade, 1999: Estimation of sea surface temperarures using GOES-8/9 radiance measurements. *Bull. Amer. Meteor. Soc.*, **80**, 1127–1137.